Research Article Vol. 35, No. 8 / August 2018 / Journal of the Optical Society of America B 1921

Journal of the Optical Society of America B

OPTICAL PHYSICS

Efficient and accurate synthesis of complex Bragg grating waveguide in dispersive silicon structures

Chenghao Feng,[1,3] Richard Soref,[2] Ray T. Chen,[3,4] Xiaochuan Xu,[3,4] and Wei Jiang[5,*]

[1]Kuangyaming Honors School, Nanjing University, Nanjing 210093, China
[2]Engineering Department, The University of Massachusetts at Boston, Boston, Massachusetts 02125, USA
[3]Department of Electrical and Computer Engineering, The University of Texas at Austin, Austin, Texas 78758, USA
[4]Omega Optics Inc., 8500 Shoal Creek Blvd., Austin, Texas 78759, USA
[5]College of Engineering and Applied Sciences, Nanjing University, Nanjing 210093, China
*Corresponding author: weijiang@nju.edu.cn

Received 3 May 2018; revised 27 June 2018; accepted 27 June 2018; posted 28 June 2018 (Doc. ID 330873); published 20 July 2018

The complex Bragg-grating waveguide (CBGW) is a semiconductor strip channel with many side corrugations or teeth. The layer-peeling (LP) and layer-adding (LA) algorithms have shown that the CBGW can be designed to offer an arbitrary pre-selected spectral-transmission profile having multiple peaks, but such a structure generally requires a huge number of teeth and a long length scale. In this paper, we propose a modified LP/LA algorithm that can significantly reduce CBGW structure length and develop accompanying time/memory-saving simulation procedures. Dispersion engineering is also introduced to significantly improve the accuracy of the LP/LA algorithm for high-index-contrast structures. A CBGW for a transmission spectrum with three passbands is designed and optimized on the silicon-on-insulator platform. Results show that our design can shorten the length of the CBGW by 10 times compared to the original design by the LP algorithm. Compared to the original LP/LA algorithm, the modified algorithm with dispersion engineering significantly improves the matching between the reconstructed transmission and the actual spectrum obtained by simulation.

OCIS codes: (130.5296) Photonic crystal waveguides; (130.4815) Optical switching devices; (230.7408) Wavelength filtering devices; (130.0250) Optoelectronics.

https://doi.org/10.1364/JOSAB.35.001921

1. INTRODUCTION

The complex Bragg-grating waveguide (CBGW) consists of a sequence of side corrugations or lateral "teeth" on a strip channel waveguide [1], as illustrated in Fig. 1. The semiconductor teeth (made of the same material as the channel) usually have the same shape on both sides of the strip, but the length, width, and sequence of individual teeth can be arbitrary. As a result, this waveguide "filter" with suitably designed teeth can have a complicated multi-peak transmission profile as a function of wavelength. The field of arbitrary CBGWs has great untapped potential in terms of rich possibilities of structure designs and broad application opportunities. CBGWs could be fabricated from semiconductor material in any of the three principal integrated-photonic network platforms based upon Si or InP or SiN. Monolithic foundry manufacture should be feasible, and the resulting structures would have medium- or high-index contrast. Currently, relatively few papers have studied CBGW in the high-index-contrast silicon photonics platform [2,3]. Knowing the fabrication, the customized complex waveguides could then be applied to several important photonic functions, such as the creation of 1) matched filters for trace-gas sensing of CH_4, CO, NH_3, etc. [4], 2) resonant thermo-optic and electro-optic 2 × 2 switches [5,6], 3) sideband filters for microwave photonics, and 4) on-chip instrumentation systems, such as refractometers, spectrometers, and Fourier-transform analyzers [7].

CBGWs constitute a new aspect of photonic integrated circuits, and CBGWs offer unique characteristics compared to other 1D photonic crystal waveguides such as narrow-band Bragg-grating waveguides (NBGWs) [8] and nanobeams [9]. Although light can be guided, confined, and controlled by those other structures, they are unable to achieve an arbitrary transmission spectrum. The CBGW is not a periodic structure; it can be seen as a NBGW with teeth widths that vary along the direction of light propagation, as per Fig. 1. Those widths are calculated with certain algorithms when the target transmission is given. If we treat the change of index variations of these NBGWs as discrete, there are algorithms such as layer peeling

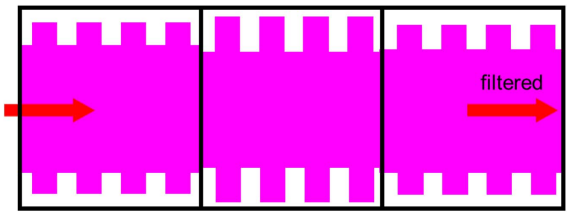

Fig. 1. Schematic drawing of complex Bragg-grating waveguide (top view) constructed in a single-mode strip waveguide (of uniform thickness) and designed to offer an optical filter transmission profile that matches an arbitrary pre-selected spectral profile. This illustrative example contains three normal Bragg grating waveguide (NBGW) segments. Each segment is illustrated by a black box that surrounds it.

(LP) [10–13]. There are several other algorithms if we treat those variations as pseudo-continuous [14–18]. The pioneering work of Zhu *et al.* [1,19] on the LP algorithm has created a highly capable computer-based electromagnetic design tool that can be used to produce a chosen multiple-peak transmission spectrum. The complicated spectral pattern of transmission that is specified at the outset of the work (the filter) is then actualized using a dedicated tooth array. CBGW has been shown to be of great use in astrophysics. Hawthorn showed that hydroxyl (OH) emission from the atmosphere can be filtered out using a complex Bragg grating in a fiber platform [20].

However, there are presently obstacles to CBGW development. For example, a 2 cm long CBGW filter could need days or weeks to calculate a single transmission wavelength [19]. The long length of CBGW devices found in early simulations seems to make them less competitive than other photonic crystal devices. This begs the question of how to reduce the device length and complexity to reach the same transmission spectrum. Because of the CBGW's length scale and complicated structure, optimization methods such as setting Bloch boundary conditions fail to work [21].

In this work, we introduce a novel approach that can significantly reduce the filter length without affecting its performance compared to those obtained by conventional LP/layer-adding (LP/LA) algorithms. In our approach, after the initial design by the conventional LP algorithm, a large number of non-essential grating segments in the spatial domain are first uncovered and removed, by virtue of physics insight from phase-related analysis. Then the remaining essential segments are used to reconstruct the spectrum using the LA algorithm. As such, the length of the CBGW is reduced significantly, which is advantageous for practical applications.

In this work, we are interested in developing CBGW on the silicon photonics platform. This leads to another important aspect of this work: developing a CBGW design method that can accommodate large index contrast and stronger dispersion in silicon waveguides. While in some lower-index-contrast systems or single narrow-band cases [2] the dispersion may be neglected, this is generally not the case in silicon-based CBGWs, as we shall see. Dispersion engineering of the complex reflection coefficients is introduced to account for the actual reflection characteristics in silicon-on-insulator (SOI)-based CBGW. Comparison between results using original LP/LA algorithms and our modified LP/LA algorithm shows the effectiveness of our approach. In addition, exploiting the periodicity within each NBGW, a transfer matrix/S-matrix-based approach is developed that substantially reduces simulation times in the reconstruction process. Our approach significantly speeds up the design/simulation compared to classic simulation approaches. To show the advantage of our approach and reveal the potential of CBGW devices, a filter with multiple passbands is designed. With our approach, the length scale is reduced 10 times compared to conventional designing methodology.

2. THEORETICAL APPROACH

A. Theoretical Background

In this subsection, we briefly review the common LP/LA algorithms used in CBGW design. The LP algorithm is a kind of inverse scattering approach. The target transmission/reflection spectrum is given first. Then the whole structure is divided into small segments with different physical parameters. Due to causality, the parameters of the first segment can be obtained according to the target reflection spectrum of the structure. Furthermore, the reflection coefficient of the second segment will be found using the extracted parameters of the first segment and the target reflection spectrum. The procedure is then repeated until the parameters of the last segment are found [11–13].

To design CBGW by the LP algorithm, we start with modeling of a normal Bragg grating waveguide since a CBGW can essentially be treated as the combination of NBGW segments, and such combined segments are indicated schematically in Fig. 1—albeit, there with a more complex teeth pattern than actually employed in the narrowband case. The modeling here is based on coupled mode theory [22]. It is well known that a NBGW has a periodic variation of the refractive index [23]. This perturbation can be expressed as

$$n(z) = n_0 + \Delta n_1 \cos\left(\frac{2\pi}{\Lambda} z + \theta_1(z)\right) + \Delta n_2 \cos\left(\frac{4\pi}{\Lambda} z + \theta_2(z)\right)\ldots, \tag{1}$$

where n_0 is the average effective refractive index, Δn_1 is the first-order perturbation to the effective refractive index, θ_i is an optical phase factor, and $\Lambda = \lambda_{\text{center}}/n_0$ is the period of the Bragg waveguide. With coupled mode theory, the transfer matrix of a NBGW can be obtained [24–26].

Then serval approximations are made. First, the operation wavelength range of target transmission shape design in the CBGW is approximated as a constant. The operation bandwidth of a CBGW is the same as the bandwidth of each NBGW segment, which is the bandwidth between the first nulls around the main reflection peak in a NBGW. It can be determined by $\Delta\lambda = \frac{\lambda_{\text{center}}^2}{\pi n_g}\sqrt{|q|^2 + (\frac{\pi}{\Delta L})^2}$, where ΔL is the length of each NBGW segment, q is the coupling coefficient [27], and n_g is the group index. For a NBGW with short periods (small ΔL) or small coupling coefficient, the operation wavelength range is

$$\Delta\lambda \approx \frac{\lambda_{\text{center}}^2}{n_g \Delta L}. \tag{2}$$

Second, it is assumed that the reflectivity of operation wavelengths is the same as that of the central wavelength. In this region, we define the reflectivity of the central wavelength as a new term, $\rho = -\tanh(|q|\Delta L)\frac{q^*}{|q|}$. It is called the complex reflection coefficient [12].

Given these approximations, the transfer matrix T of the NBGW can be simplified and rewritten [11,12]. When different Bragg gratings of different index variations are put in series, the change of reflection field between two adjacent NBGWs has a certain relation. The relation can be expressed as a formula with two expressions. We call them LP/LA algorithms. The two equations are shown below. The whole grating has a total length L and is divided into N individual segments, $\rho(z)$ is the complex reflection coefficient of the nth segment, and $z = n\Delta L$. $r(z, \delta)$ is the reflectivity at position (z) when the wavenumber detuning is δ:

$$r(z + \Delta L, \delta) = \exp(-i2\delta\Delta L)\frac{r(z, \delta) - \rho(z)}{1 - \rho^*(z) r(z, \delta)}, \tag{3}$$

$$r(z, \delta) = \frac{r(z + \Delta L, \delta) + \rho(z)\exp(-i2\delta\Delta L)}{\exp(-i2\delta\Delta L) + \rho^*(z) r(z + \Delta L, \delta)}. \tag{4}$$

Equation (3) is the equation of LP, while Eq. (4) is the equation of LA [1,12,13]. Their usages will be explained later.

Before the designing procedures, the phases of each wavelength in the target reflection should be given, and they should be physically realizable. In spectrum design, only the target transmission power |T| is known, while the phase of the field is not given. If we perform an inverse Fourier transform on target reflection $r(z = 0, \delta)$ in the frequency domain, we get the impulse response of reflection in the time domain $r(z = 0, t)$. Physically, the reflection occurs only after an input light enters the device when $t = 0$. Therefore, the impulse response of reflection should be zero when $t < 0$ in the time domain. To realize this, a window function is usually operated on the reflection to force the field reflection r to be zero when $t < 0$ [1,12,13]. The phase of reflection is given too because of the window function.

The conventional designing process is the following: First, $r(z = 0, \delta) = \sqrt{R(z = 0, \delta)} = \sqrt{1 - T(\delta)}$ is given; then the complex reflection coefficient of the first segment $\rho(z = 0)$ is obtained using

$$\rho(z) = \frac{1}{M}\sum_{-\delta_\omega/2}^{\delta_\omega/2} r(z, \delta), \tag{5}$$

where M is the number of wavelengths used in target transmission, and δ_ω is the designed spectrum width of CBGW in wavenumber space. Equation (7) can be deduced by discrete Fourier transform [12]. Then the reflectivity of the second segment $r(z = \Delta L, \delta)$ is calculated by Eq. (2), while the complex reflectivity coefficient $\rho(z = \Delta L)$ is obtained from $r(z = \Delta L, \delta)$ with Eq. (4). After that, the reflectivity and reflectivity coefficient of the third segment $r(z = 2\Delta L, \delta)$ $\rho(z = 2\Delta L)$ are calculated again using Eqs. (2) and (4). The whole process is iterated until the $\rho(z)$ is found for all the NBGW segments. In the end, a mapping process is done to transform $\rho(z)$ to the geometry structure of each segment using the relations between $\rho(z)$ and effective index variations [12,13].

LA was used to reconstruct the transmission only to check whether the calculated transmission matches our target transmission in previous papers. In this paper, we show that it can also be employed as a powerful tool for optimizing the structure. More details about LP/LA algorithms can be found in the papers of Skaar and Feced [12,13].

B. Design Optimization Methods

From the basic LP/LA theory, many parameters, including L, ΔL, n_0, and filter structure parameters can be set by us. This leaves us a lot of space to explore designs that satisfy our requirements but that use the simplest and shortest possible structure. However, optimizing structures requires an understanding of the LP/LA mechanisms.

From $L = N\Delta L$, the length scale is determined by the number of NBGW segments N and the length of each NBGW segment Δ. N is also the number of iterations in the LP algorithm. To reduce the length scale, we want as few segments as possible to design the filter with target transmission. Hence, the number of iterations should be controlled, and the iteration efficiency should be improved.

In designs, we find that the iteration efficiency is related to the magnitude of $\rho(z)$, for it determines the change of the reflection when reconstructing the reflection. It is obvious from Eqs. (2), (3), and (5) that when $\rho(z) \to 0$, the grating can be seen as a normal waveguide and $r_{(z,\delta)} \to r_{(z+\Delta L,\delta)} e^{i2\delta\Delta L}$, which means that the reflection changes only its phase in this segment. From the LP algorithm, if $\rho(z) = \frac{1}{M}\Sigma r(z, \delta) \to 0$, in the next iteration, $\rho(z + \Delta L) \approx \frac{1}{M}\Sigma r(z, \delta)^{-i2\delta\Delta L} \to 0$. The iterations in LP are not efficient with small $\rho(z)$; however, the inefficient iterations are common in structures designed by the LP algorithm. Window functions, say, the Hanning window function, is routinely operated upon r_{target} to shift the original reflected impulse in order to force the reflected impulse to be nonzero only when $t > 0$. Thus, $\rho(z = 0) = \frac{1}{M}\Sigma r_{\text{target}}(\delta) = \rho(t = 0) \to 0$, as deduced by an inverse Fourier transform. On the other hand, there is no backward propagation field at the end of the filter, $\rho(z = L) = 0$. As a result, the reflection will evolve slowly with slowly changing ρ at the beginning or the end of the filter.

In order to solve the problem of inefficient iterations, we suggest cutting the head and the tail of the filter designed by the LP method and to keep only the central parts where $\rho(z)$ evolves rapidly. The reflection and transmission of the selected parts can be calculated with the LA method to check whether the reconstructed reflection will retain its shape with much smaller length scale. In this way, the LA algorithm is used not only to reconstruct and check the transmission but also to select and optimize the useful part of the filter designed by LP. Figure 2 shows the comparison between the transmission of 1000 segments and 100 segments after selecting the central part. The designed transmission has a 10 nm rectangle-shaped passband centered at $\lambda_0 = 1550$ nm. After selecting the central 100 segments only [460th to 559th segments from the original 1000 segments in Fig. 2(b)], the target bandwidth

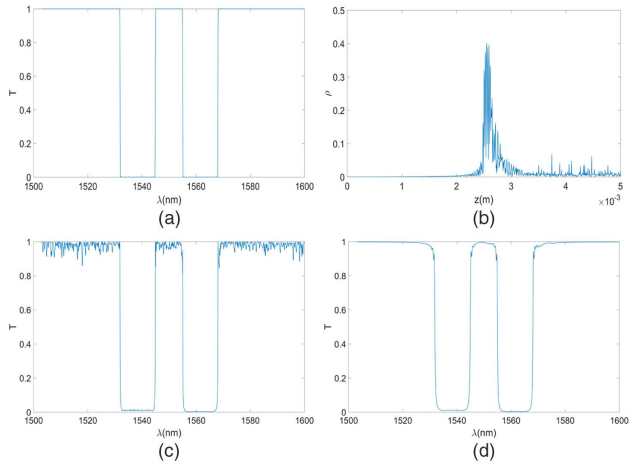

Fig. 2. (a) Target transmission. (b) Calculated ρ (z) after the target transmission is given. 1000 segments are used. The total length is 5 mm. (c) Calculated transmission of 1000 segments. (d) Calculated transmission using only the central 100 segments. The optimized length is 500 um. The selected part is from $z = 2.3$ mm to $z = 2.8$ mm in (b).

(BW) and central wavelength are preserved. The transmission of the optimized design is even smoother than the original design. Using Eq. (3), designers can flexibly adjust the design calculated by the LP algorithm and optimize the filter to a compact size for practical applications.

C. Simulation Optimization Methods

After finishing the designing process and getting the $\rho(z)$ of each segment, we need to find the structure that has such $\rho(z)$s and simulate the transmission spectrum of our structure to test the validity of our designs. In each NBGW segment, the index variation is described by Eq. (1). A mapping process needs to be performed to get the physical structure of the CBGW for simulation and fabrication. The mapping process is performed using the finite difference eigenmode (FDE) solver of Lumerical Mode Solutions. Each NBGW segment is divided into many teeth of different widths to map index variations. It should be noted that the relationship between the teeth width and the effective index is not linear.

There will be numerous structures to choose from in order to approximate the sinusoidal index variations. As in the NBGW, teeth are needed to build a CBGW. The number of teeth we use in one period of index variation will decide the total number of teeth utilized, which can be approximated by the following equation:

$$N_{\text{teeth}} \approx \frac{L}{\Lambda} * N_{\text{period}} = \frac{N\Delta L}{\Lambda} * N_{\text{period}}, \tag{6}$$

where N_{period} is the number of teeth we use in a period of index variations.

The coupling coefficient of the NBGW derived from the coupled mode theory [Eq. (1)] $\kappa = \frac{\pi\Delta n}{2\lambda_0}$ is valid only in weak Bragg gratings [27]. For high-index-contrast silicon waveguide gratings, we need to obtain the relation between $\rho(z)$ and teeth corrugations or index perturbation directly from finite difference time domain (FDTD) simulations. It is known that

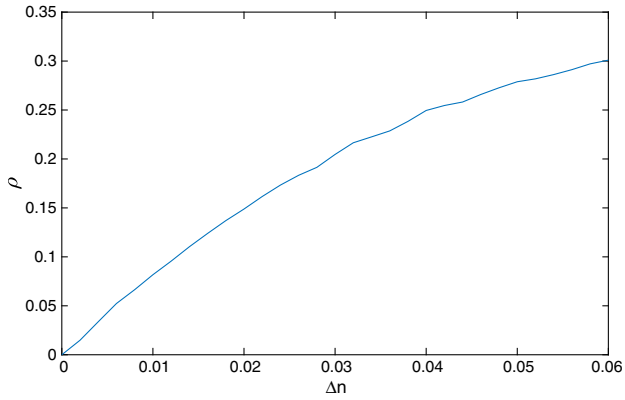

Fig. 3. Relation between effective index perturbation and reflectivity of NBGW ρ. Each NBGW has 20 periods. The average effective index is 2.48.

$\rho(z)$ is the reflectivity of the NBGW from previous deductions. One can simulate NBGWs with different teeth corrugations with a fixed average effective index, get the reflectivity, and then use methods such as interpolation to get the relation. Figure 3 gives an example when the average effective index is fixed to be 2.48. In this way, strong Bragg gratings can also be applied in CBGW design.

After assembling the teeth, the device needs to be simulated to predict its performance. However, direct FDTD simulation of a long filter with an extremely large number of teeth (e.g., 200,000 in Ref. [1]) requires prohibitive memory and time in computing.

Using current solvers in 3D simulation software, we explored ways to reduce simulation time and memory. We arrived at the method of simulating each NBGW segment, then obtaining the transfer matrix of all segments, and then reconstructing the S matrix instead of simulating the whole structure. Given that each segment is a NBGW, a periodic structure, the eigenmode expansion (EME) solver will be ideal to deal with segments. The time we save depends on the number of periods in one segment. For instance, if one uses NBGW segments that contain 32 periods in each, then the simulation time based on our optimization method will be at least 32 times faster than simulating the whole structure using EME/FDTD, not to mention the acceleration gained because of the memory we save. Note that only one period in each segment is needed to be stored in the memory in any procedure we use.

D. Dispersion Engineering

During the simulations, it is common to find that the simulated transmission is far from the reconstructed transmission by the LP algorithm. The reason is that the equations of LP/LA are based on theoretical assumptions from previous sections. Some assumptions/approximations may be invalid for silicon waveguides, which have higher index contrast and relatively large dispersion.

First, it is easy to note that a large difference between the group index and the effective index exists in silicon waveguides, whereas in a fiber grating or SiN waveguide, such a dispersion effect can be neglected by interchangeable use of n_g and n_0

[28,29]. For a $250 * 450$ nm silicon waveguide, the group index when $\lambda = 1550$ nm is 4.3, while the effective index is only 2.4. If we use the original LP/LA algorithm for silicon waveguides and introduce the difference between n_g and n_0, the final spectrum will be narrower than our designed spectrum.

Second, considering the change of reflection in operation wavelengths is essential, especially in short-period Bragg gratings. In CBGW design, we hope to use short-period segments to reduce the length scale. However, the reflection of a NBGW is not rectangle shaped in the wavelength domain. The transmission of wavelengths far from central wavelengths will match badly with numerical calculations if the reflection variations are not considered. Such a larger spectral range requires us to consider the more complex dispersion effect—the wavelength dependence of $\rho(z)$.

Here, we suggest rewriting $\rho(z)$ as

$$\rho(z,\lambda) = \rho(z) \times \frac{f(\lambda)}{|\rho(z)|}, \tag{7}$$

where $f(\lambda)$ presents the frequency response of a NBGW. For a grating with fixed Bragg wavelength, $f(\lambda)$ is affected mainly by wavelength detuning from the Bragg wavelength and by the dispersion of the silicon waveguide for short-period (small ΔL) gratings. From simulations shown in Fig. 4, both amplitude and phase of $f(\lambda)$ with certain periods are similar with different index perturbations, and they can be introduced into the original LP/LA algorithms. The shapes of $f(\lambda)$ from sample NBGWs with different index perturbations are shown in Fig. 4. It can be seen that the reflectivity is declining with increasing wavenumber detuning. This is common, for there does not exist a distinct boundary between the zero-transmission region and the transmitted region, especially for short-period NBGW. The slight errors caused by neglecting $f(\lambda)$ will bring disastrous results after hundreds of iterations. For example, if 100 segments are used, the error when $\lambda = 1549$ nm is $0.99^{100} = 0.37$. Since the shapes of $f(\lambda)$ are similar, we suggest using one interpolated function to fit $f(\lambda)$, and then introducing $f(\lambda)$ to Eqs. (5) and (6). The original $\rho(z)$ is replaced by $\rho(z,\lambda)$. LP and LA become wavelength dependent. The design will be better controlled in this way.

To summarize this section, our optimization is to design an appropriate target $T(\lambda)$, and to get also the target reflection spectrum $r(0,\delta)$ and then to calculate the $\rho(z)$, which determines coupling coefficients one by one using the modified LP algorithm. After the initial structure design is done, modified LA is used to reconstruct and check the transmission and to select useful parts of initial structures to reduce L. After that, we map the effective index variations to appropriate physical structures. Finally, the physical structure is simulated in a short time. Tradeoffs need to be made between device performances and device length scales.

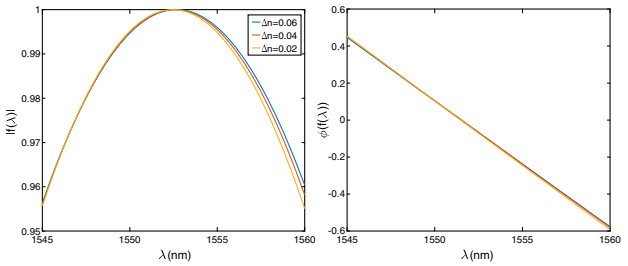

Fig. 4. $f(\lambda)$ of different NBGWs. The left is the amplitude of $f(\lambda)$, and the right is the phase of $f(\lambda)$. Each NBGW has 20 periods. The average effective index is 2.48. The index variations are 0.02, 0.04, and 0.06, respectively.

3. RESULTS AND DISCUSSION

In this section, we demonstrate that a CBGW with multiple passbands can be designed in SOI at 1550 nm, and the bandwidth of each passband can be controlled with our modifications. The NBGWs we use have a period of $\Lambda = 312$ nm, and the central wavelength of them is controlled to be 1552.5 nm. The thickness of the waveguide is 250 nm, and the width W of Si in Fig. 1 is 450 nm.

As an example, we select a three-passband filter with different bandwidths to demonstrate arbitrary control of both the center wavelength and the bandwidth of each peak. The first peak is $\lambda_1 = 1549$ nm with 1.5 nm BW, the second is $\lambda_2 = 1552.5$ nm with 1 nm BW, and the third is $\lambda_3 = 1555$ nm with 0.5 nm BW. The bandwidths of each passband and the spacing between any two peaks are different.

For initial tests, a "long" waveguide was selected; then the central part is selected as our final design. One thousand NBGW segments, each 6.2 μm in length, were used in the initial design. Once those parameters were set, $\rho(z)$ of each NBGW segment was calculated by the LP algorithm, After that, the LA algorithm was used to optimize the structure and then reconstruct the transmission. After examining the reconstructed transmission, the central 100 segments are picked up as our final design. The final length scale is 624 um. The structure is designed on the SOI platform with SiO_2 upper cladding of the CBGW. The outer widths of the silicon region (core plus grating teeth) of these 100 segments are shown in Fig. 5. The average refractive index of each segment is fixed.

Figure 6 shows the comparison between the target transmission, the reconstructed transmission using the whole 6.2 mm structure, and the optimized final 624 μm structure using the LA algorithm. We can see that the basic properties of the multi-band filter, including locations of passbands, bandwidth,

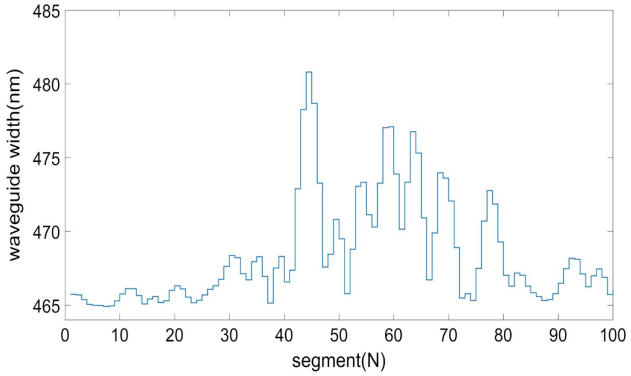

Fig. 5. Grating structures of the our final CBGW design. It has 100 segments. The silicon region's outer width (core plus grating teeth) of each segment is shown.

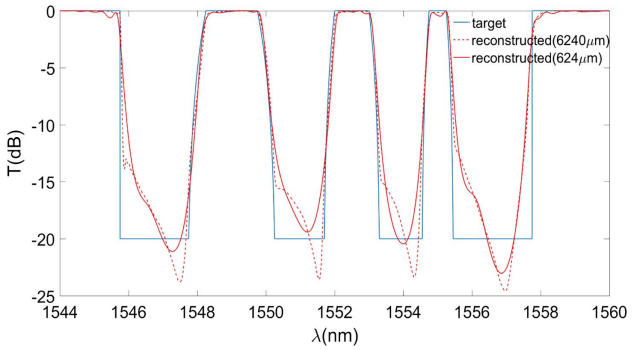

Fig. 6. Comparison between target transmission (blue solid) and reconstructed transmission of the original 6.24 mm structure (red dashed), using LA, and the reconstructed transmission of the optimized 624 um structure.

and band-rejection depth, are controlled with the optimized structure. The length scale has been shortened 10× compared to the original design.

Figure 7 shows that the EME simulation results of the structure designed by the modified LP/LA algorithms match well with the reconstructed spectrum calculated by the LA algorithm. It can be seen that the transmission shape designed by modified LP/LA algorithms is similar to the reconstructed transmission spectrum. It reveals that the results attained by solving Maxwell equations rigorously fits well with our numerical calculations using Eq. (6). We attribute the small gap between simulation results and calculation results using Eq. (6) to the effects not considered in the transfer matrix of NBGW, such as small errors due to approximations mentioned above in the mapping process. Figure 8 shows the group delay of our transmission in our final CBGW design. The phase response can be obtained by integrating group delay.

Note that there will be some modal mismatch between adjacent NBGW segments. The EME-based transfer matrix method has already included the modal mismatch effect within its computational framework. However, the original LP/LA

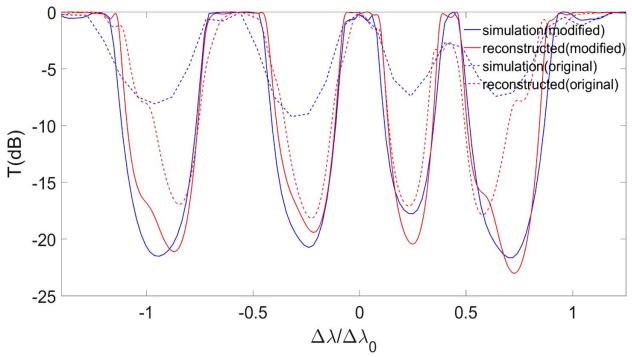

Fig. 7. Comparison between simulation result of the filter designed by modified LP/LA (blue solid) and its reconstructed spectrum (red solid). The simulated spectrum (blue dashed) and the reconstructed spectrum (red dashed) of the filter designed by the original LP/LA algorithm (blue dashed) are also shown for comparison. The horizontal wavelength axis is given by $\Delta\lambda/\Delta\lambda_0 = (\lambda - \lambda_2)(\lambda_3 - \lambda_1)$. The two blue curves are obtained by the EME simulation.

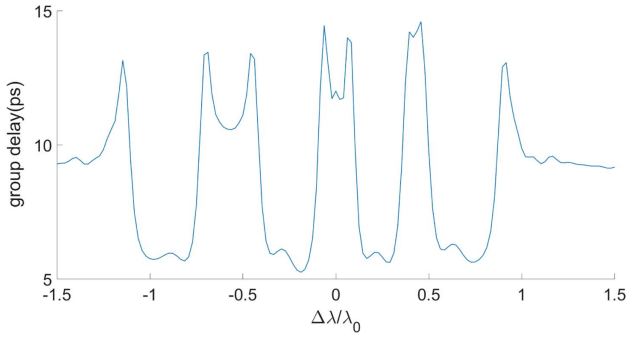

Fig. 8. Group delays of the transmission simulated by EME solver. The horizontal wavelength axis is the same as that in Fig. 7.

algorithm appears to neglect the modal mismatch, as it tends to be small (the teeth widths are less than 4% of the waveguide width).

Simulation and reconstruction results of the filter designed by original LP and LA algorithms are also shown in Fig. 7. Due to omission of dispersion in the original LP/LA algorithm, the reconstructed spectrum departs significantly from the simulated spectrum of the structure. Furthermore, the extinction ratios of the stopbands are poor (especially in the simulated spectrum). It is because the reflectivity of wavelengths away from the central wavelength is overestimated in the original LP/LA algorithms. As a consequence, not enough light in the stopband region is reflected in the filter. It is worth mentioning that low extinction ratios similar to the original LP have been observed in single-band SOI grating waveguides [2]. Here, we show that both the locations of the bands and their profiles in the reconstructed spectrum agree accurately with the spectrum designed by the modified LP/LA method. Note that today's advanced CMOS fabrication technology is capable of controlling line-width variation (not feature size) on the order of >2 nm [30]. Our simulation shows that the transmission spectral profile changes ∼1 dB over the simulated wavelength range if those shallow grating teeth <2 nm are omitted, which indicates our structure can be fabricated in CMOS foundries.

4. CONCLUSION

We have presented a general computer-assisted approach to the design and optimization of complex Bragg-grating channel waveguides.

The basic structures of the filter will be given by the LP algorithm. Optimization of the structure can be implemented by the LA algorithm. Success has been had here by reducing the number of segments comprising the overall length L without injuring the filter quality. Methods for space- and-time-efficient simulations are also given here.

Considering the dispersion of silicon waveguides and the frequency response of NBGWs, a dispersive form of the complex reflection coefficient is introduced. The method of calculating such coefficients has been developed. Also, attention has been paid to differentiate the phase index and group index in various equations.

Finally, we have performed modeling and simulation of a filter with multiple passbands. The comparison between the

original LP/LA and the modified LP/LA shows that significant improvement in the accuracy of the spectral profile can be obtained with the modified LP/LA algorithms.

Overall, the modified LP/LA algorithms significantly reduce the structure length and simulation time/computer memory. Dispersion engineering improves the accuracy of designing a spectrum profile for multi-band systems.

Funding. National Key R&D Program of China (2017YFA0303700, 2017YFA0303704); Keys and Joan Curry/Cullen Trust Endowed Chair; National Natural Science Foundation of China (NSFC) (61775094, 41427801); Fundamental Research Funds for the Central Universities (021314380072).

Acknowledgment. C. F. wishes to thank the Lumerical support team and Dr. Swapnajit Chakravarty for their advice on simulations. R. S. acknowledges the support of the AFOSR.

REFERENCES

1. T. Zhu, Y. Hu, P. Gatkine, S. Veilleux, J. Bland-Hawthorn, and M. Dagenais, "Arbitrary on-chip optical filter using complex waveguide Bragg gratings," Appl. Phys. Lett. **108**, 101104 (2016).
2. A. D. Simard, M. J. Strain, L. Meriggi, M. Sorel, and S. Larochelle, "Bandpass integrated Bragg gratings in silicon-on-insulator with well-controlled amplitude and phase responses," Opt. Lett. **40**, 736–739 (2015).
3. A. D. Simard and S. LaRochelle, "Complex apodized Bragg grating filters without circulators in silicon-on-insulator," Opt. Express **23**, 16662–16675 (2015).
4. W. C. Lai, S. Chakravarty, X. Wang, C. Lin, and R. T. Chen, "On-chip methane sensing by near-IR absorption signatures in a photonic crystal slot waveguide," Opt. Lett. **36**, 984–986 (2011).
5. H. Zhou, H. Qiu, X. Jiang, Q. Zhu, Y. He, Y. Zhang, and R. Soref, "Compact, submilliwatt, 2 × 2 silicon thermo-optic switch based on photonic crystal nanobeam cavities," Photon. Res. **5**, 108–112 (2017).
6. J. Hendrickson, R. Soref, J. Sweet, and W. Buchwald, "Ultrasensitive silicon photonic-crystal nanobeam electro-optical modulator: design and simulation," Opt. Express **22**, 3271–3283 (2014).
7. H. Podmore, A. Scott, P. Cheben, A. V. Velasco, J. H. Schmid, M. Vachon, and R. Lee, "Demonstration of a compressive-sensing Fourier-transform on-chip spectrometer," Opt. Lett. **42**, 1440–1443 (2017).
8. T. E. Murphy, J. T. Hastings, and H. I. Smith, "Fabrication and characterization of narrow-band Bragg-reflection filters in silicon-on-insulator ridge waveguides," J. Lightwave Technol. **19**, 1938–1942 (2001).
9. S. R. Tutorial, "Integrated-photonic switching structures," APL Photon. **3**, 021101 (2018).
10. S. Paul, T. Saastamoinen, S. Honkanen, M. Roussey, and M. Kuittinen, "Multi-wavelength filtering with a waveguide integrated phase-modulated Bragg grating," Opt. Lett. **42**, 4635–4638 (2017).
11. A. Buryak, J. Bland-Hawthorn, and V. Steblina, "Comparison of inverse scattering algorithms for designing ultrabroadband fibre Bragg gratings," Opt. Express **17**, 1995–2004 (2009).
12. J. Skaar, L. Wang, and T. Erdogan, "On the synthesis of fiber Bragg gratings by layer peeling," IEEE J. Quantum Electron. **37**, 165–173 (2001).
13. R. Feced, M. N. Zervas, and M. A. Muriel, "An efficient inverse scattering algorithm for the design of nonuniform fiber Bragg gratings," IEEE J. Quantum Electron. **35**, 1105–1115 (1999).
14. D. T. H. Tan, K. Ikeda, R. E. Saperstein, B. Slutsky, and Y. Fainman, "Chip-scale dispersion engineering using chirped vertical gratings," Opt. Lett. **33**, 3013–3015 (2008).
15. V. Veerasubramanian, G. Beaudin, A. Giguere, B. Le Drogoff, V. Aimez, and A. G. Kirk, "Design and demonstration of apodized comb filters on SOI," IEEE Photon. J. **4**, 1133–1139 (2012).
16. M. J. Strain, S. Thoms, D. S. MacIntyre, and M. Sorel, "Multi-wavelength filters in silicon using superposition sidewall Bragg grating devices," Opt. Lett. **39**, 413–416 (2014).
17. X. Wang, W. Shi, R. Vafaei, N. A. F. Jaeger, and L. Chrostowski, "Uniform and sampled Bragg gratings in SOI strip waveguides with sidewall corrugations," IEEE Photon. Technol. Lett. **23**, 290–292 (2011).
18. M. Verbist, W. Bogaerts, and D. Van Thourhout, "Design of weak 1-D Bragg grating filters in SOI waveguides using volume holography techniques," J. Lightwave Technol. **32**, 1915–1920 (2014).
19. T. Zhu, "Layer peeling/adding algorithm and complex waveguide brag grating for any spectrum generation & fiber-to-waveguide coupler with ultra high coupling efficiency," doctoral dissertation (University of Maryland, 2016).
20. J. Bland-Hawthorn, S. C. Ellis, S. G. Leon-Saval, R. Haynes, M. M. Roth, H. G. Löhmannsröben, and P. A. Gillingham, "Complex multi-notch astronomical filter to suppress the bright infrared sky," Nat. Commun. **2**, 581 (2011).
21. J. D. Joannopoulos, S. G. Johnson, J. N. Winn, and R. D. Meade, *Photonic Crystals: Molding the Flow of Light* (Princeton University, 2011).
22. A. Yariv, "Coupled-mode theory for guided-wave optics," IEEE J. Quantum Electron. **9**, 919–933 (1973).
23. M. Kulishov, J. M. Laniel, N. Bélanger, J. Azaña, and D. V. Plant, "Nonreciprocal waveguide Bragg gratings," Opt. Express **13**, 3068–3078 (2005).
24. X. Daxhelet and M. Kulishov, "Theory and practice of long-period gratings: when a loss becomes a gain," Opt. Lett. **28**, 686–688 (2003).
25. R. Kashyap, *Fiber Bragg Gratings* (Academic, 1999), Chap. 4.
26. T. Erdogan, "Fiber grating spectra," J. Lightwave Technol. **15**, 1277–1294 (1997).
27. X. Wang, *Silicon Photonic Waveguide Bragg Gratings* (University of British Columbia, 2013).
28. J. M. C. Boggio, D. Bodenmüller, T. Fremberg, R. Haynes, M. M. Roth, R. Eisermann, M. Lisker, L. Zimmermann, and M. Böhm, "Dispersion engineered silicon nitride waveguides by geometrical and refractive-index optimization," J. Opt. Soc. Am. B **31**, 2846–2857 (2014).
29. http://refractiveindex.info/?group=CRYSTALS&material=Si3N4.
30. ITRS, International Technology Roadmap for Semiconductors, 2000, www.itrs2.net.